Facilitation of Ferroelectric Switching via Mechanical Manipulation of Hierarchical Nanoscale Domain Structures

Zibin Chen,[1] Liang Hong,[2,†] Feifei Wang,[3] Simon P. Ringer,[1,4] Long-Qing Chen,[2] Haosu Luo,[5] and Xiaozhou Liao[1,*]

[1]*School of Aerospace, Mechanical and Mechatronic Engineering, The University of Sydney, Sydney, New South Wales 2006, Australia*

[2]*Department of Materials Science and Engineering, Pennsylvania State University, University Park, Pennsylvania 16802, USA*

[3]*Key Laboratory of Optoelectronic Material and Device, Department of Physics, Shanghai Normal University, Shanghai 200234, China*

[4]*Australian Institute for Nanoscale Science and Technology, The University of Sydney, New South Wales 2006, Australia*

[5]*Key Laboratory of Inorganic Functional Materials and Devices, Shanghai Institute of Ceramics, Chinese Academy of Sciences, Shanghai 200050, China*

(Received 14 June 2016; revised manuscript received 4 October 2016; published 6 January 2017)

Heterogeneous ferroelastic transition that produces hierarchical 90° tetragonal nanodomains via mechanical loading and its effect on facilitating ferroelectric domain switching in relaxor-based ferroelectrics were explored. Combining *in situ* electron microscopy characterization and phase-field modeling, we reveal the nature of the transition process and discover that the transition lowers by 40% the electrical loading threshold needed for ferroelectric domain switching. Our results advance the fundamental understanding of ferroelectric domain switching behavior.

DOI: 10.1103/PhysRevLett.118.017601

Ferroelectric materials, exhibiting intrinsic coupling of spontaneous polarization and strain, have been extensively investigated for their critical applications in next-generation logical devices, nonvolatile memories, actuators, and sensors [1–5]. A low-threshold field for ferroelectric domain switching is important for advanced applications for low energy consumption. Lowering the threshold field requires a comprehensive understanding of domain switching kinetics under external stimuli, including temperature [6,7], electrical bias [8–14], and/or mechanical stress [15–17]. Recent investigations demonstrated that domain orientation has significant effects on the polarization hysteresis, coercive field, remanent polarization, and dielectric and piezoelectric properties of ferroelectric materials under electrical bias stimulation [18–20]. These effects can result from the fact that the nucleation barrier of ferroelastic domain walls is small along some specific directions, leading to a high density of ferroelastic domain walls that promotes ferroelastic transition and, consequently, facilitate ferroelectric transition [13].

Previous investigations of domain switching kinetics were usually conducted using epitaxial ferroelectric films [21–23]. While ferroelectric switching in the film can be facilitated by ferroelastic transition, it usually requires delicate selection of a crystalline direction and proper design of the epitaxial ferroelectric films [18,21], including the selection of the substrate and film materials and film thickness. Further, the motion of the ferroelastic domain walls in epitaxial thin films is usually restricted by the elastic constraint of the substrate that limits the ferroelastic transition [24]. In bulk ferroelectric materials without constraint by any substrate, the formation of freely mobile ferroelastic domain walls requires relatively low energy, making it possible to promote ferroelectric switching via ferroelastic transition [25,26]. Therefore, it will be of significant interest to explore a controllable way of manipulating a high density of freely mobile ferroelastic domain walls and to understand the microscopic mechanism of the interaction of ferroelastic and ferroelectric switching in bulk ferroelectrics.

Recent development in *in situ* transmission electron microscopy (TEM) has provided a platform for applying simultaneously multiple stimuli on micro- and nanoscale specimens [8,24,27], measuring their physical and mechanical properties, and studying the structural evolutions under the external stimuli. This makes it possible to conduct a real-time examination of polarization switching. In this Letter, we applied *in situ* TEM and phase-field modeling to investigate a heterogeneous ferroelastic transition process (coexistence of ferroelastic nano- and microdomains) by applying mechanical loading and to explore its significant impact on assisting ferroelectric transition under simultaneous mechanical and electrical loading in Pb $(Mg_{1/3}Nb_{2/3})O_3$-38%$PbTiO_3$ (PMN-38%PT) single crystals with tetragonal domains [28] at room temperature. The formation of a high density of tetragonal domains in normal ferroelectrics usually requires biaxial constraint in thin films [27,29]. This limits significantly the motion of

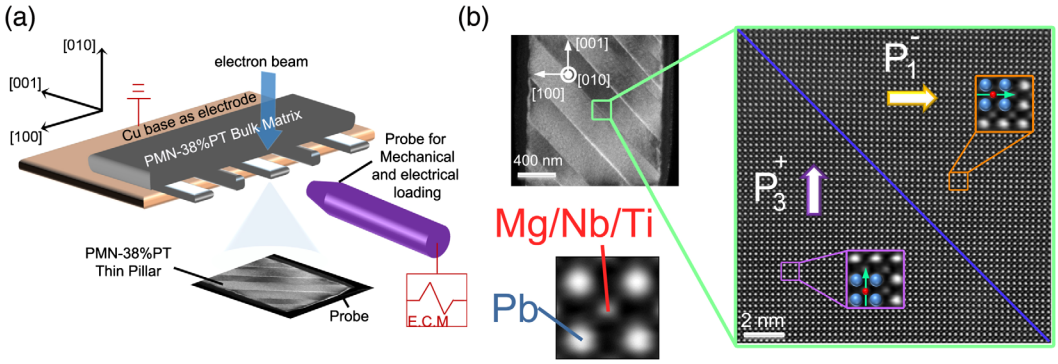

FIG. 1. (a) Schematic diagram of the experimental setup. A bulk PMN-38%PT matrix with thin pillars was fixed on a grounded Cu platform using Pt deposition. A conductive tip connected to the electrical characterization module (ECM) acts as an indenter and electro for mechanical and electrical loading. The actual allocation of the pillar and the tip was captured in the enlarged TEM image. (b) A dark-field TEM image and an STEM-HAADF image showing a head-to-tail tetragonal domain configuration across a domain boundary as indicated in the green box. The domain wall is indicated using the blue line while polarizations are indicated using large purple and yellow vectors. The inset purple and yellow boxes show the enlarged polarizations in the P_3^+ and P_1^- domain area, respectively.

ferroelastic domain walls. For relaxor-based ferroelectric PMN-38%PT, the energy barriers for domain nucleation and motion within tetragonal domains are expected to be significantly lower than those of normal ferroelectrics, e.g., $PbTiO_3$ and $PbZr_{0.2}Ti_{0.8}O_3$, because it is close to the morphotropic phase boundary of PMN-xPT [26]. As a result, it is possible to have a high density of 90° ferroelastic domains in a PMN-38%PT single crystal without being biaxially constrained in thin films. Our phase-field simulations and *in situ* TEM observations demonstrated a decreased threshold value of external electric field for ferroelectric switching through the manipulation of ferroelastic 90° nanodomains by mechanical loading. These results significantly advance our fundamental understanding on how mechanical loading assists polarization reversal and provide a new way for the manipulation of a high density of mobile ferroelastic domain walls in bulk single crystals.

Figure 1(a) presents a schematic of the *in situ* experimental setup. A bulk PMN-38%PT single crystal was fixed on a Cu base using Pt deposition. Multiple PMN-38%PT pillars with dimensions of 2.0 μm × 1.3 μm × 0.08 μm (length × width × thickness) were produced using mechanical grinding followed by focused ion-beam processing. *In situ* mechanical and electrical stimuli were applied by a conductive probe in TEM. The Cu base acted as one electrode and the conductive probe as the other electrode. A typical domain configuration observed from a pillar is presented in Fig. 1(b). Lamellarlike domains with bandwidths of hundreds of nanometers in 45° inclination were found in the pillar. The atomic-resolution scanning TEM (STEM) high-angle annular dark-field (HAADF) technique was used to image polarization directions and domain wall structures. Figure 1(b) shows an example of an HAADF image in which a domain wall that separates the head-to-tail tetragonal domains was marked by a blue solid line. All domains in the pillar were examined, confirming the overall head-to-tail domain orientation in the pillar.

In this Letter, tetragonal domains with polarization along the positive and negative [100], [010], and [001] axes are referred to as P_1^+, P_1^-; P_2^+, P_2^-; and P_3^+, P_3^-, respectively. Through the measurement of the displacement between Pb cations and their surrounding Mg/Nb/Ti cations in the HAADF image in Fig. 1(b)[30], the polarizations of the domains on the left (P_3^+) and right (P_1^-) sides of the domain wall were determined pointing towards [001] and [$\bar{1}$00], respectively [see the details in the enlarged purple and orange boxes in Fig. 1(b)]. The structure of the alternating head-to-tail 90° domains with straight P_3^+-P_1^- domain walls inside the initial domain configuration in this PMN-38%PT single crystal pillar is, therefore, identified.

Domain switching processes in the PMN-38%PT single crystal pillar under separately applied electrical or mechanical loadings were investigated. To simplify the discussion, details of the electrical loading effect are presented in the Supplemental Material S1 [31]. Electrical loading led to 180° ferroelectric domain reversal in the tetragonal microdomains but did not alter the ferroelastic domain structure. Generally, the nucleation energy barrier of ferroelastic 90° domain walls is lower than that of ferroelectric 180° domain walls in single crystals without a significant pinning force to 90° domain walls [13,43]. However, our experimental results shown in S1 suggested a ferroelectric switching rather than the motion of ferroelastic domain walls. Therefore, there could be a relatively strong pinning effect to the ferroelastic microdomain walls in the present PMN-38%PT single crystal, which would originate from the existence of oxygen vacancy, topological defects, or compositional variation in relaxor-based ferroelectrics [44–47].

Domain switching under mechanical loading presents a markedly different picture from electrical loading. Figures 2(a)–2(e), which are extracted from Supplemental Material, movie 1 [31], show the evolution of domain

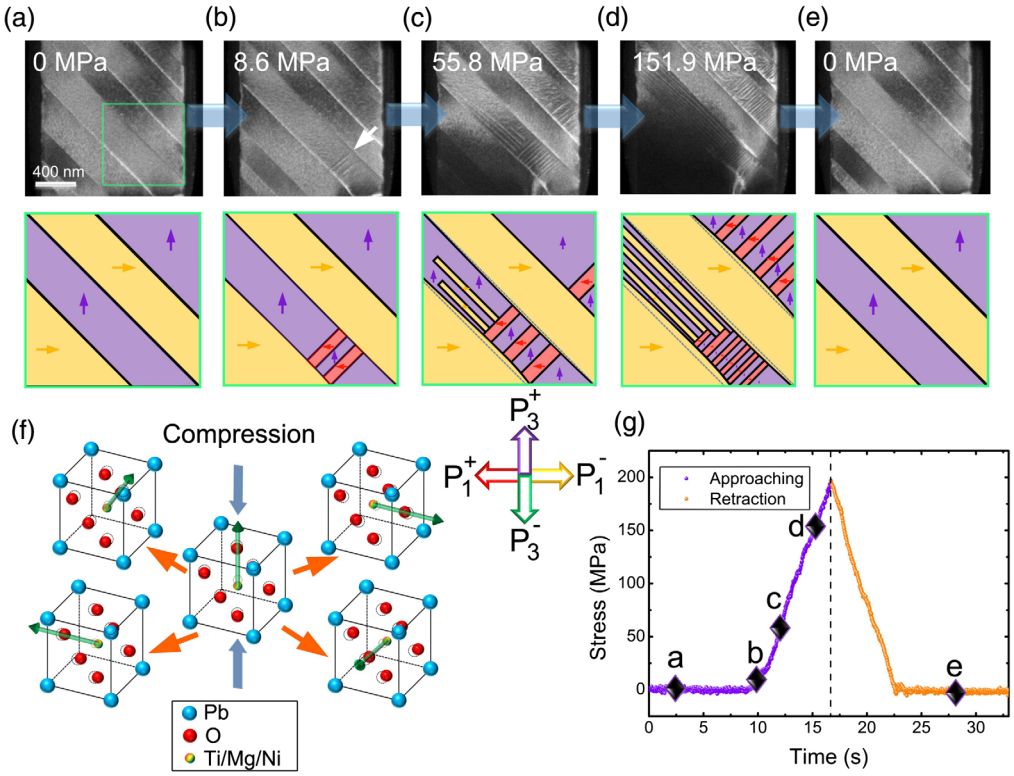

FIG. 2. (a)–(e) A series of images showing the evolution of ferroelastic domains under mechanical excitation. At the bottom of each image is the schematic drawing of the domain structure in the area within the green box indicated in (a). (f) Schematic of the introduction of four possible types of polarization by applying compression along [001] to the original polarization along [001]. (g) A load or bias versus time curve showing the real-time application of mechanical load with zero bias. Labels (a) to (e) correspond to the image order from (a) to (e) and indicate their relative position in the curve.

configurations during a mechanical loading cycle [Fig. 2(g)]. The domain configurations in the green box area [see Fig. 2(a)] at different stress stages are schematically illustrated in the lower part of Figs. 2(a)–2(e). The initial domain configuration with alternate P_3^+ and P_1^- domains is shown in Fig. 2(a). At the stress level of 8.6 MPa, some straight nanobands with the orientation perpendicular to the original P_3^+-P_1^- domain wall formed, as indicated by the white arrow in Fig. 2(b).

Analysis of the newly formed structures (see Supplemental Material [31], S2) indicates that the straight bands are new P_1^+ domains with a charge neutral head-to-tail 90° P_3^+-P_1^+ wall perpendicular to the original microdomain walls as illustrated in the lower part of Fig. 2(b) in red. Upon increasing the stress to 55.8 MPa, straight bands with orientation parallel to the original microdomain walls formed as shown in Fig. 2(c). The straight nanobands parallel to the microdomain walls are newly switched P_1^- domains with P_3^+-P_1^- domain walls. Our experimental results show that the original microdomain wall positions, as indicated by the dotted lines in the lower part of Fig. 2(c), shifted slightly through shrinkage of the P_3^+ domains. While the motion of the microdomain walls is limited with further increasing the stress, the density of new nanodomains increased dramatically [Fig. 2(d)]. Once the external stress was removed, the switched domain fully reversed where the new nanodomains disappeared and the microdomain walls returned to their original positions [Fig. 2(e)]. Note that the original P_1^- domains remained unchanged during the mechanical loading cycle, because P_1^- domains are the favorable ones under compression along [001] as schematically shown in Fig. 2(f). Since the pillar was close to a two-dimensional material with significant (010) surfaces, the polarization switching to P_2^+ and P_2^- would induce significant electrostatic field, which is not favorable and, therefore, was not detected in the experiment. Figure 2(g) shows the corresponding loading stress-time curve. Because the loading and unloading processes were displacement control with a constant displacement rate, the approximate linear stress-time curve for approaching and retraction indicates that the deformation process of the pillar was elastic without obvious bending.

The application of mechanical loading significantly modified the domain orientation, which could affect the electrical poling process. Macroscopic studies on mechanical loading with electrical poling [48] reported that the electric-field–polarization hysteresis as well as the ferroelectric properties are completely different from the ones with electrical poling only. Such difference is significant when

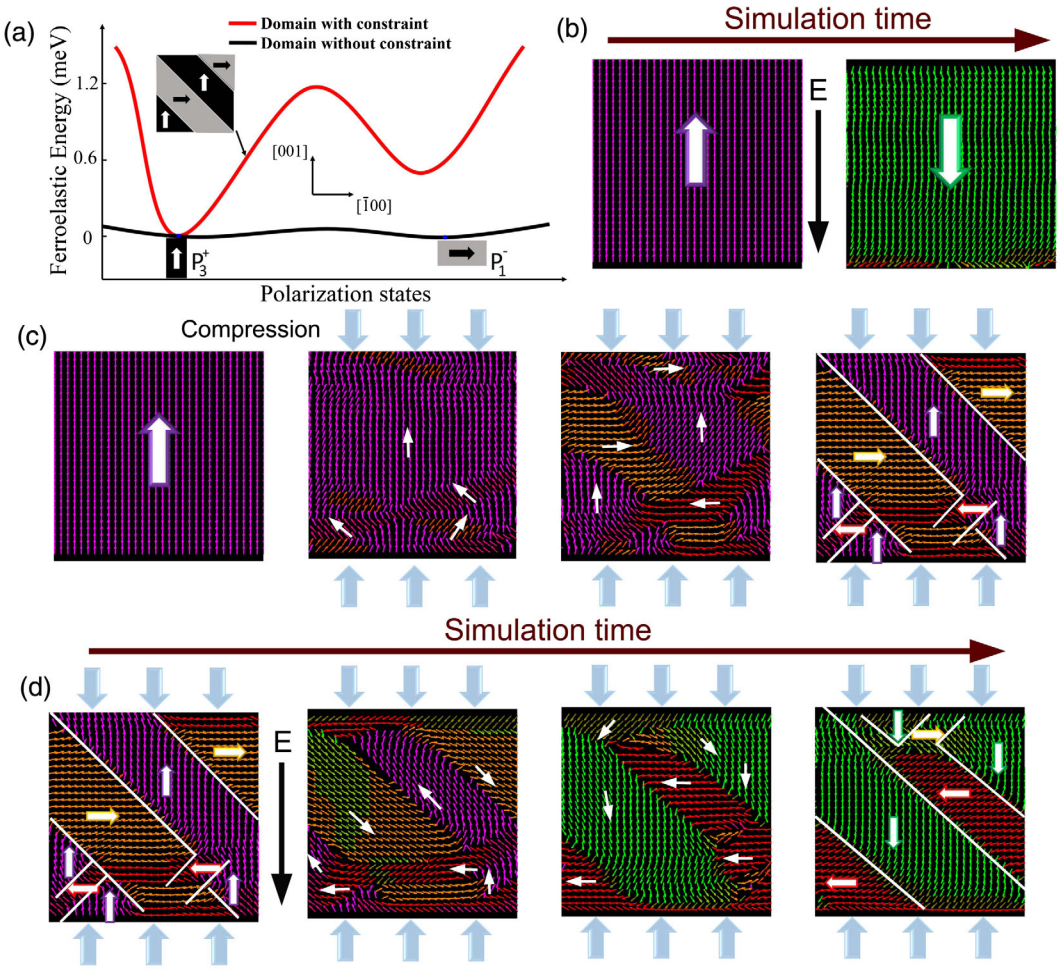

FIG. 3. Phase-field simulation and calculation on kinetic domain transformation in PMN-38%PT single crystal. (a) Predicted ferroelastic energy of tetragonal domains in a PMN-38%PT single crystal. Two local minimum points in the wavy red curve represent the ferroelastic energy for a constrained c domain and a domain, respectively. The local maximum in the middle of the red curve represents the energy required (energy barrier) for rotating a single c domain to an a domain. (b),(c),(d) Domain transition under electrical loading only, mechanical loading only, and combined mechanical and electrical loading, respectively.

the compressive stress is larger than 20 MPa. A possible mechanism was proposed that all P_3^+ domains were converted to a single P_1^- domain through the motion of the original P_3^+-P_1^- microdomain walls with mechanical loading over 20 MPa [48,49]. However, our experimental results showed otherwise. With the pinned ferroelastic microdomain walls and relatively low energy barriers for domain nucleation and motion within microdomains, compressive stress favored the formation of a high density of ferroelastic 90° nanodomains inside the P_3^+ microdomains, indicating that the difference in electrical poling dynamic is due to the formation of 90° nanodomains.

Figure 3 presents results of the phase-field calculations and simulations on the domain transition kinetics in a PMN-38%PT single crystal under different loading conditions. In order to demonstrate the pinning effect of microdomain walls on domain transition kinetics, we first calculated the ferroelastic energy of tetragonal domains with and without constraint (details of the phase-field calculations and simulations are described in Supplemental Material [31]). Figure 3(a) shows that while the ferroelastic energy for a c domain remains the same, the ferroelastic energy barrier for rotating a single c domain (P_3 domian) to an a domain (P_1 domian) with constraint is 1 order of magnitude larger than that without constraint. Therefore, the elastic energy can be easily relaxed when the microdomain is not constrained by neighboring domain walls. In contrast, domain transition in a P_3^+ microdomain, whose elastic expansion or contraction along [100] is constrained by the pinned P_3^+-P_1^- microdomain walls, occurs via the formation of intermediate ferroelastic domains. The large elastic energy barrier for the constraint situation not only leads to the formation of an intermediate ferroelastic 90° domain structure but also presents an approach for reversible ferroelastic switching after external mechanical stress is removed.

When only an electrical loading is applied to a single P_3^+ domain, ferroelectric 180° domain switching (P_3^+ to P_3^-) occurs [Fig. 3(b)], which requires little elastic energy change. When only mechanical stress is applied, multiple ferroelastic 90° P_1 domains are produced in the pillar as shown in Fig. 3(c). If the compression is removed, most P_1 domains rotate back to the original tetragonal P_3^+ domain, demonstrating the reversible ferroelastic domain transition, which is consistent with the experimental observation shown in Fig. 2 and the calculated ferroelastic energy barrier presented in Fig. 3(a).

The above simulation results explain very well the formation of the 90° tetragonal nanodomains shown in Fig. 2. During the mechanical loading, the motion of microdomain walls is limited by the pinning effects, leading to constraint on P_3^+ microdomains. The resulting significant elastic energy tends to be released instantly through the formation of multiple nanosized P_1 domains.

Figure 3(d) presents the effect of the formation of ferroelastic nanodomains on ferroelectric switching under combined mechanical and electrical loading by phase-field simulations. The initial state was the stable domain structure under mechanical loading shown in Fig. 3(c). Keeping the same mechanical loading, electrical loading was applied along the P_3^- direction, resulting in a fundamentally different domain switching evolution. Instead of rotating towards the poling direction, tetragonal domains rotate 90° only, i.e.,$P_3^+ \rightarrow P_1^-$, $P_1^+ \rightarrow P_3^-$, and $P_1^- \rightarrow P_3^-$. With combined mechanical and electrical loadings, the ferroelectric switching proceeds via ferroelastic domain transition, and all domain walls keep charge neutral, which minimizes electrostatic fields.

The 90° domain switching with the assistance of high-density 90° tetragonal nanodomains is revealed by phase-field simulations for combined electrical and mechanical loading. An *in situ* TEM study on the domain switching process under combined mechanical and electrical loading was also conducted to confirm the phase-field prediction. The combined loading was applied to the same pillar used in Fig. S1 [31]. A negative bias of −4 V was first applied to completely recover the initial domain structures shown in Fig. S1a (see Supplemental Material [31], S4) and Fig. 4(a). Then, mechanical loading of 190 MPa along the [001] direction was applied, forming two new types of 90° nanodomain walls as shown in Fig. 4(b). The mechanical stress was maintained during the subsequent electrical loading process. The domain structures in each distinct domain subband type shown in Figs. 4(a)–4(d) were presented schematically in Figs. 4(e)–4(l).

At the initial state [Fig. 4(a)], the domain subband in area (e) is up-poled (P_3^+). With the mechanical stress, parts of P_3^+ rotate to P_1^+ [with P_3^+-P_1^+ domain walls in (f)] and P_1^- [with P_3^+-P_1^- domain walls in (g)]. By applying +3 V electrical bias while keeping the same mechanical loading [Fig. 4(c)], 90° reorientation of domain boundaries occurred in both the (h) and (i) domain subbands, while the domain boundaries in (j) did not change. The 90° domain wall rotation from (f) and (g) to (h) and (i), respectively, are intermediate states that facilitate the whole 180° domain wall rotation by electric loading under mechanical loading. Without mechanical loading, such 90° domain wall rotation would occur only when the electrical poling is along the [111] direction [18].

Such interesting continuous rotation of 90° tetragonal nanodomain structure under combined electrical and mechanical excitations is closely related to the ferroelastic transition. Without mechanical loading, 180° domain reversal takes place with the formation of charge neutral 180° domain walls. Surprisingly, it is found that (f) rotates 90° to (h) when an electrical bias is applied as shown in Fig. 4(c). Similarly, (g) rotates 90° to (i) [Fig. 4(c)] followed by another 90° domain wall rotation to (k) with the increase of the bias [Fig. 4(d)]. According to the phase-field simulations shown in Fig. 3(d), the (g) state rotating to the (k) state via orthorhombic domains is an energetically favorable path when only charge neutral domain walls exist. However, accompanying with the existence of the pinned neighboring P_1^- domain, the P_3^+-P_1^- (g) nanodomain walls energetically prefers rotating 90° [to (i)] towards P_1^- before reaching the energetically favorable state (k). Once the state (k) is stabilized, the significantly charged domain wall between (k) and the original P_1^- microdomain will rotate the neighboring P_1^- domains to P_1^+. The transition from (f) to (h) is also attributed to the same reason, in which the neighbor switched P_1^+ domain stabilized the (h) state, making it difficult to rotate again. This is confirmed from the switching process in Fig. 4 that the neighboring 180° P_1^--P_1^+ domain wall, indicated by white arrow in Fig. 4(d), keeps the same pace with the production of stable P_3^--P_1^+ domain structure [(h) and (k)]. It is also noted that such stable 90° nanodomain structure (P_3^--P_1^+) is consistent with our phase-field simulation results. Further increasing the electric field would ultimately lead to (l) → (m) switching.

Since ferroelastic switching requires less external energy than ferroelectric switching [43,50], electronic devices that realize ferroelectric switching via controllable ferroelastic transition are more energy efficient. The length of switched domains is an important parameter for examining ferroelectric properties, including coercive field, remanent polarization, and the electromechanical coupling factor [51]. Figure 4(n) shows the length of switched domains as a function of electric bias. The maximum switched P_3^- domain length for combined electrical and mechanical loadings was significantly larger than that without mechanical loading. The domain switching was initiated at bias of +2 and +3.2 V, respectively, for the situations with and without mechanical loading. The former is surprisingly ~40% lower than the latter. Nevertheless, the switched P_1^+ domain lengths (inset

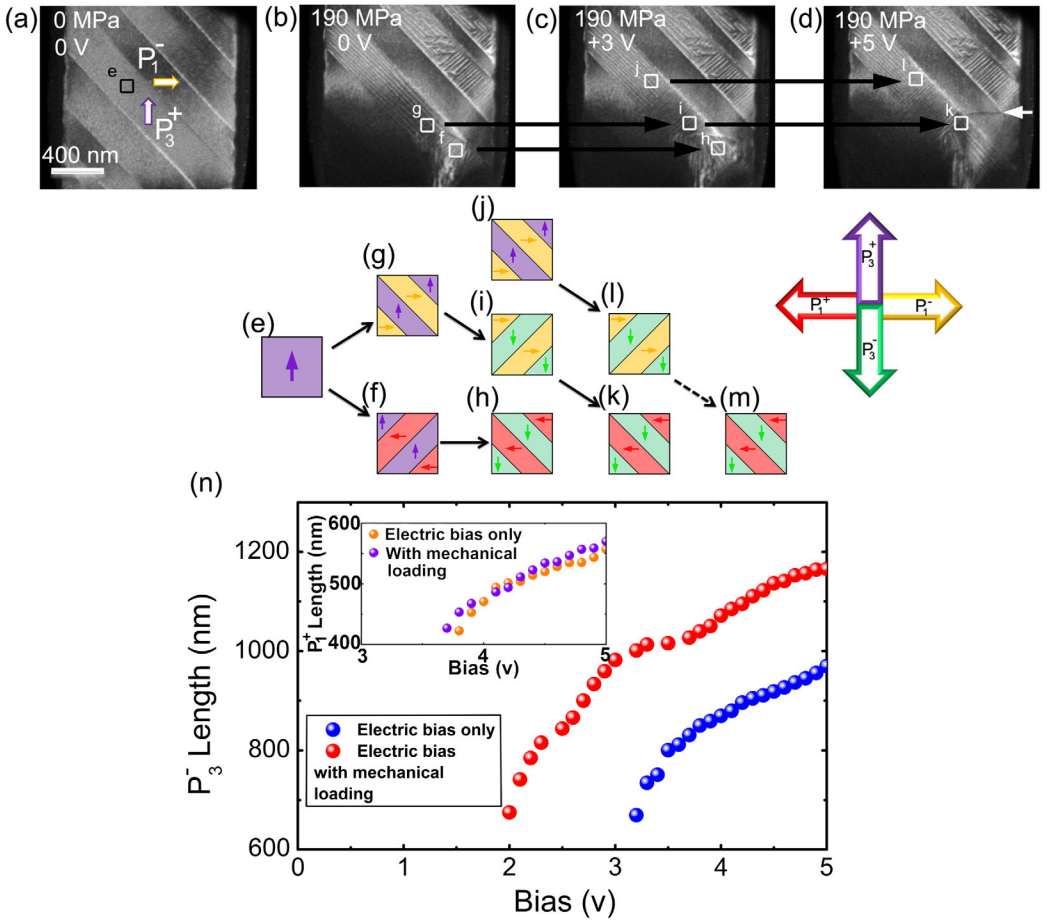

FIG. 4. (a)–(d) A series of experimental images (extracted from the Supplemental Material [31], movie 3) showing the evolution of ferroelastic domains under electrical loading with mechanical loading. The 180° ferroelectric domain wall P_1^+-P_1^- is indicated by the white arrow in (d). (e)–(k) illustrations of the switching process in an originally P_3^+ microdomain, for the initial state (e), mechanical loading only (f),(g), low electrical bias with mechanical loading (h)–(j), high electrical bias with mechanical loading (k),(l), and predicted higher electric bias with mechanical loading (m). (n) Switched domain length verses bias graph comparing the domain switching capabilities of electrical loading with and without mechanical loading in P_3^+ microdomains and P_1^- microdomains (the inset graph).

graph) were almost identical for both cases because there was no switching assistance from 90° nanodomains in the P_1^- microdomains.

In summary, our *in situ* electron microscopy experiments and phase-field simulations revealed the domain switching processes of ferroelectric PMN-38%PT single crystals under different external loading conditions. Hierarchical ferroelastic domain transition was found when significant mechanical stress was applied. Phase-field simulations confirmed the experimental observations that the 90° ferroelastic transition takes place under electrical poling with mechanical loading, while 180° tetragonal microdomain reversal occurs under electrical loading without mechanical loading. The formation of 90° nanodomains assists ferroelectric domain switching and reduces the threshold field for the domain switching by 40%, indicating the unique role mechanical loading plays during the electrical poling. This study provides new insights into achieving a controllable ferroelastic transition to facilitate ferroelectric switching in bulk ferroelectric materials.

The authors are grateful for the scientific and technical support from the Australian Microscopy & Microanalysis Research Facility node at the University of Sydney and the assistance of Dr. David Mitchell of the Electron Microscopy Centre of the University of Wollongong. This research was financially supported by the Australian Research Council. The work at Penn State was supported by the U.S. Department of Energy, Office of Basic Energy Sciences, Division of Materials Sciences and Engineering under Award No. FG02-07ER46417. This research was supported by the Faculty of Engineering & Information Technologies, The University of Sydney, under the Faculty Research Cluster Program.

Z. C. and L. H. contributed equally to this work.

*To whom all correspondence should be addressed. Xiaozhou.liao@sydney.edu.au

†Present address: Department of Materials Science and Nanoengineering, Rice University, Houston, Texas 77005, USA.

[1] V. Garcia and M. Bibes, Nature (London) **483**, 279 (2012).
[2] B. H. Park, B. S. Kang, S. D. Bu, T. W. Noh, J. Lee, and W. Jo, Nature (London) **401**, 682 (1999).
[3] E. W. Sun and W. W. Cao, Prog. Mater. Sci. **65**, 124 (2014).
[4] C. B. Eom and S. Trolier-McKinstry, MRS Bull. **37**, 1007 (2012).
[5] D. Lee, S. Mo Yang, T. Heon Kim, B. C. Jeon, Y. Su Kim, J.-G. Yoon, H. N. Lee, S. Hyup Baek, C. B. Eom, and T. W. Noh, Adv. Mater. **24**, 402 (2012).
[6] S. C. Chae, N. Lee, Y. Horibe, M. Tanimura, S. Mori, B. Gao, S. Carr, and S. W. Cheong, Phys. Rev. Lett. **108**, 167603 (2012).
[7] A. K. Singh, D. Pandey, and O. Zaharko, Phys. Rev. B **74**, 024101 (2006).
[8] Y. Sato, T. Hirayama, and Y. Ikuhara, Phys. Rev. Lett. **107**, 187601 (2011).
[9] M. G. Han, Y. M. Zhu, L. J. Wu, T. Aoki, V. Volkov, X. Y. Wang, S. C. Chae, Y. S. Oh, and S. W. Cheong, Adv. Mater. **25**, 2415 (2013).
[10] C. T. Nelson *et al.*, Science **334**, 968 (2011).
[11] P. Gao *et al.*, Adv. Mater. **24**, 1106 (2012).
[12] M. P. Cruz, Y. H. Chu, J. X. Zhang, P. L. Yang, F. Zavaliche, Q. He, P. Shafer, L. Q. Chen, and R. Ramesh, Phys. Rev. Lett. **99**, 217601 (2007).
[13] S. H. Baek *et al.*, Nat. Mater. **9**, 309 (2010).
[14] Z. Chen, X. Wang, S. P. Ringer, and X. Liao, Phys. Rev. Lett. **117**, 027601 (2016).
[15] W. J. Chen, Y. Zheng, W. M. Xiong, X. Feng, B. Wang, and Y. Wang, Sci. Rep. **4**, 5339 (2014).
[16] H. Lu, C. W. Bark, D. E. de los Ojos, J. Alcala, C. B. Eom, G. Catalan, and A. Gruverman, Science **336**, 59 (2012).
[17] K. Kim and J. E. Huber, J. Eur. Ceram. Soc. **35**, 1459 (2015).
[18] R. J. Xu, S. Liu, I. Grinberg, J. Karthik, A. R. Damodaran, A. M. Rappe, and L. W. Martin, Nat. Mater. **14**, 79 (2015).
[19] D. Damjanovic, F. Brem, and N. Setter, Appl. Phys. Lett. **80**, 652 (2002).
[20] J. Peng, J. Z. Chen, H. S. Lu, T. H. He, H. Q. Xu, and D. Lin, Solid State Commun. **130**, 53 (2004).
[21] J. C. Agar *et al.*, Nat. Mater. **15**, 549 (2016).
[22] L. F. Chen, Z. H. Cheng, W. T. Xu, X. J. Meng, G. L. Yuan, J. M. Liu, and Z. G. Liu, Sci. Rep. **6**, 19092 (2016).
[23] D. J. Kim, J. Y. Jo, Y. S. Kim, Y. J. Chang, J. S. Lee, J. G. Yoon, T. K. Song, and T. W. Noh, Phys. Rev. Lett. **95**, 237602 (2005).
[24] P. Gao *et al.*, Nat. Commun. **5**, 3801 (2014).
[25] E. K. H. Salje, in *Annual Review of Materials Research*, edited by D. R. Clarke (Annual Reviews, Palo Alto, 2012), Vol. 42, p. 265.
[26] Z. Wang, R. Zhang, E. W. Sun, and W. W. Cao, J. Appl. Phys. **107**, 014110 (2010).
[27] P. Gao, J. Britson, J. R. Jokisaari, C. T. Nelson, S. H. Baek, Y. R. Wang, C. B. Eom, L. Q. Chen, and X. Q. Pan, Nat. Commun. **4**, 2791 (2013).
[28] Y. Zhang, D. Z. Xue, H. J. Wu, X. D. Ding, T. Lookman, and X. B. Ren, Acta Mater. **71**, 176 (2014).
[29] C. S. Wang *et al.*, Nat. Commun. **7**, 10636 (2016).
[30] C. L. Jia, V. Nagarajan, J. Q. He, L. Houben, T. Zhao, R. Ramesh, K. Urban, and R. Waser, Nat. Mater. **6**, 64 (2007).
[31] See Supplemental Material at http://link.aps.org/supplemental/10.1103/PhysRevLett.118.017601 for additional information on how ferroelectric domains and ferroelastic domains evolute under mechanical and electrical stimulations, the materials synthesis and characterization, and the method of the phase-field model, which includes Refs. [32–42].
[32] J. Wang, S. Q. Shi, L. Q. Chen, Y. L. Li, and T. Y. Zhang, Acta Mater. **52**, 749 (2004).
[33] I. Vrejoiu, G. Le Rhun, N. D. Zakharov, D. Hesse, L. Pintilie, and M. Alexe, Philos. Mag. **86**, 4477 (2006).
[34] X. J. Lou and J. Wang, J. Appl. Phys. **108**, 034104 (2010).
[35] T. Choi, Y. Horibe, H. T. Yi, Y. J. Choi, W. D. Wu, and S. W. Cheong, Nat. Mater. **9**, 253 (2010).
[36] L. Q. Chen, Annu. Rev. Mater. Res. **32**, 113 (2002).
[37] L. Q. Chen, J. Am. Ceram. Soc. **91**, 1835 (2008).
[38] Y. L. Li, S. Y. Hu, Z. K. Liu, and L. Q. Chen, Acta Mater. **50**, 395 (2002).
[39] Ag. Khachaturyan and G. A. Shatalov, Sov. Phys. JETP **29**, 557 (1969).
[40] Y. L. Li, S. Y. Hu, Z. K. Liu, and L. Q. Chen, Appl. Phys. Lett. **81**, 427 (2002).
[41] L. Hong, A. K. Soh, Q. G. Du, and J. Y. Li, Phys. Rev. B **77**, 094104 (2008).
[42] Y. M. M. Jin, Y. U. Wang, and A. G. Khachaturyan, Philos. Mag. **83**, 1587 (2003).
[43] S. Liu, I. Grinberg, and A. M. Rappe, Nature (London) **534**, 360 (2016).
[44] Y. Nahas, S. Prokhorenko, I. Kornev, and L. Bellaiche, Phys. Rev. Lett. **116**, 127601 (2016).
[45] F. Chu, I. M. Reaney, and N. Setter, J. Am. Ceram. Soc. **78**, 1947 (1995).
[46] P. Paruch and J. Guyonnet, C.R. Phys. **14**, 667 (2013).
[47] R. C. Smith and C. L. Hom, J. Intell. Mater. Syst. Struct. **10**, 195 (1999).
[48] S. Patel, A. Chauhan, and R. Vaish, J. Appl. Phys. **117**, 084102 (2015).
[49] K. G. Webber, R. Z. Zuo, and C. S. Lynch, Acta Mater. **56**, 1219 (2008).
[50] B. Meyer and D. Vanderbilt, Phys. Rev. B **65**, 104111 (2002).
[51] G. Catalan, A. Schilling, J. F. Scott, and J. M. Gregg, J. Phys. Condens. Matter **19**, 132201 (2007).